nature energy

Resource

https://doi.org/10.1038/s41560-024-01620-9

Multi-year field measurements of home storage systems and their use in capacity estimation

Received: 13 December 2023

Accepted: 26 July 2024

Published online: 16 September 2024

Check for updates

Jan Figgener[1,2,3,4,5] ✉, Jonas van Ouwerkerk[1,2,3,4,5], David Haberschusz[1,2,3,4,5], Jakob Bors[2,3,5], Philipp Woerner[2,3], Marc Mennekes[2,3,5], Felix Hildenbrand[1,2,3,4], Christopher Hecht[1,2,3,4], Kai-Philipp Kairies[2,3,5], Oliver Wessels[2,3] & Dirk Uwe Sauer[1,2,3,4,5,6]

Home storage systems play an important role in the integration of residential photovoltaic systems and have recently experienced strong market growth worldwide. However, standardized methods for quantifying capacity fade during field operation are lacking, and therefore the European batteries regulation demands the development of reliable and transparent state of health estimations. Here we present real-world data from 21 privately operated lithium-ion systems in Germany, based on up to 8 years of high-resolution field measurements. We develop a scalable capacity estimation method based on the operational data and validate it through regular field capacity tests. The results show that systems lose about two to three percentage points of usable capacity per year on average. Our contribution includes the publication of an impactful dataset comprising approximately 106 system years, 14 billion data points and 146 gigabytes, aiming to address the shortage of public datasets in this field.

The market for home storage systems has been growing strongly over the past years[1]. To make the investment of around 10,000 € per system[1] more appealing, manufacturers give warranty periods of 10 years. However, the industry lacks standardized state of health (SOH) evaluations[2], and customers have to rely on the given values of battery management systems (BMSs), which have unknown calculation schemes[2] and inaccuracies[3]. To establish transparency, the batteries regulation of the European Union requires reliable and transparent SOH estimations[4]. Therefore, methods to determine the SOH of battery storage systems in field operation are urgently needed.

In the laboratory, methods to determine the SOH are defined to a large extent. Laboratory measurements are based on monitoring individual cells in a controlled environment, which are aged by either cycling[5–14] or storing them[5,8,15,16] at specific conditions. The ageing within these tests is tracked via regular capacity measurements, and results vary depending on the investigated chemistry and testing conditions[17]. However, these tests are time-consuming[18], and real-world operation is always subject to unpredictable changes[19], which is why simulations of field operation are applied in the laboratory[20–22].

Field capacity tests can be found for grid storage[23–25], photovoltaic (PV) integration[19,26,27], telecommunication[28] and electric vehicles (EVs)[29,30]. While most of these use on-site capacity tests to monitor battery ageing[19,23–26,28], others remove the battery for laboratory measurements[24,27,29]. Such capacity tests require a certain system downtime, leading to increasing work time and decreasing revenue.

[1]Center for Ageing, Reliability and Lifetime Prediction of Electrochemical and Power Electronic (CARL), RWTH Aachen University, Aachen, Germany. [2]Institute for Power Electronics and Electrical Drives (ISEA), RWTH Aachen University, Aachen, Germany. [3]Institute for Power Generation and Storage Systems (PGS), E.ON ERC, RWTH Aachen University, Aachen, Germany. [4]Juelich Aachen Research Alliance, JARA-Energy, Aachen, Germany. [5]ACCURE Battery Intelligence GmbH, Aachen, Germany. [6]Helmholtz Institute Münster (HI MS), IMD 4, Forschungszentrum Jülich, Jülich, Germany. ✉e-mail: jan.figgener@isea.rwth-aachen.de

https://doi.org/10.1038/s41560-024-01620-9

Table 1 | Aggregated overview of the measured HSSs

Nomenclature and chemistry	Nominal energy in kWh	Inverter power in kW	Nominal voltage in V	Number of systems of one product	Aggregated number of systems
'Small$_{LMO}$' or 'S$_{LMO}$' with LMO/NMC blend battery ('LMO')	2.2	2	146.7	6	6
'Medium$_{NMC}$' or 'M$_{NMC}$' with NMC battery	8.6	2.5	50.4	1	7
	8.7	3	48.1	2	
	8.8	3	46.8	2	
	9.8	5	51.8	1	
	11.5	2.5	50.4	1	
'Medium$_{LFP}$' or 'M$_{LFP}$' with LFP batteries	8.1	3	51.2	4	8
	9.2	3.3	46	2	
	10.0	3	51.2	1	
	13.8	3.5	46	1	

About 106 system years represented by 14 billion data points totalling 146 GB were analysed.

Operational data analysis is a promising way to overcome the shortcomings of conducted field capacity tests[30–38]. The capacity-based SOH estimation is widely used to track the decreasing capacity[39]. Coulomb counting is an established approach for this but comes with several challenges, such as the required knowledge of an initial state of charge (SOC) and its sensitivity to error accumulation[40]. Therefore, different methods have been developed to estimate the SOH, which can be categorized into model-based and data-driven approaches[41]. Model-based methods[42] use either equivalent circuit models[40,43–46] or electrochemical models describing the internal electrochemical processes of the battery[47–50]. Model-based SOH estimators are mainly limited by their high computational costs, and their accuracy depends highly on the parameterization[39]. Machine learning methods do not model the internal working principles of the battery[51]. Instead, they map ageing-related input features of the battery to its SOH[42,51], using algorithms such as Gaussian process regression[52,53], support vector machines[54,55] and different types of neural network approach[39,56–58].

The lack of publicly available field measurement datasets is a problem that many studies face or explicitly identify as a general shortcoming today[2,59,60]. For example, thematical close publications of Dubarry et al.[60,61] analyse synthetical home storage system (HSS) battery data derived from measured irradiance to develop diagnostic methods using machine learning and incremental capacity analysis. The developed methods show promising results and could be validated with the dataset of this paper. Several battery datasets are accessible to the public, originating from laboratory measurements or synthetic cell simulations. Constant cycling data for varying battery chemistries and conditions can be found in refs. 11–14,62–66. Specific discharging conditions are used in refs. 67–71, where driving cycles are used to simulate the usage of the tested batteries in EV applications. Synthetic datasets simulating many degradation paths and corresponding battery data can be found in refs. 72,73. Real-world EV operational data with lithium-ion batteries was recently published[2,74] with valuable datasets[71,75]. Lead-acid solar home batteries in Africa are evaluated in ref. 76. Nevertheless, if such large field datasets are published in rare cases, there are usually no reference measurements to validate the developed algorithms. A detailed overview of public datasets is given in ref. 59.

On the basis of the conducted literature research, we conclude that first, most research focuses on EVs[2,74,77–83] and not on stationary storage systems[3,60,76]. Second, the measurement periods are usually limited to 1–2 years of operation[2,74,78–81,83], mostly without conducted validation measurements, and the datasets are typically not shared. Third, the internal resistance is regularly chosen[2,76] as a health metric, as the capacity[78] is difficult to examine during field operation and the exact origins of the stated BMS values are unknown[2,3]. However, the capacity is the most important metric for the battery lifetime and is subject to given warranties.

To contribute to battery research, this paper analyses field data of 21 privately operated HSSs of the first product generation over up to 8 years. The main scientific contributions of this paper are the development of a method to estimate the usable battery capacity of home storage systems and the publication of the large dataset. The key findings are that the measured HSSs in field operation lose about 2–3 percentage points (pp) of capacity per year. Compared with other publications, the long measurement period and periodic field capacity tests allow for method validation. Alongside the paper, we publish the dataset consisting of 106 system years, 14 billion data points and 146 gigabytes in 1,270 monthly files. To the best of our knowledge, no comparable public dataset for various lithium-ion batteries of HSSs has been used to date (year 2024) for scientific capacity estimation. We expect the dataset to enable researchers worldwide to develop new SOH estimation methods.

Dataset of 21 home storage systems over 8 years

The ISEA/CARL of RWTH Aachen University measured 21 private HSSs in Germany over up to 8 years from 2015 to 2022. All these HSSs are combined with residential PV systems to increase self-consumption. The measured quantities relevant to this paper are system-level battery current, voltage, power, battery pack housing temperature and room temperature, while the sample rate is 1 second. Table 1 contains an overview of the measured HSS batteries and their main parameters, and Supplementary Note 1 gives detailed information on the measurements in general and the high-resolution measurement systems used.

The operational behaviour of the systems is determined by two main parameters, which are the system design and the used cell chemistry. While some metrics such as the current rate (C-rate) or the number of equivalent full cycles (EFCs) depend on the system design and the ratio of battery energy to inverter power, the cell chemistries have different open circuit voltage (OCV) curves and specific ageing characteristics. Supplementary Tables 1 and 2 give more information on the system-specific quantities and the used measurement hardware. Figure 1a shows the C-rate and the cell voltage for an exemplary HSS and summer day, while Fig. 1b,c presents an overview of data availability and data gaps, which is explained in more detail in Supplementary Note 2.

The different cathode materials are lithium nickel manganese cobalt oxide (NMC), a blend of lithium manganese oxide (LMO) and NMC (simply referred to as 'LMO' in this paper), and lithium iron phosphate (LFP). Within the NMC systems, there are differences in cell chemistry. Two of the NMC systems have a high nickel share.

To account for system design and cell chemistry, the system nomenclature gives information on both parameters to interpret the results. Therefore, this paper refers to 'Small$_{LMO}$' (or 'S$_{LMO}$'), 'Medium$_{NMC}$' (or 'M$_{NMC}$') and 'Medium$_{LFP}$' (or 'M$_{LFP}$') HSSs. As there are already HSSs in the energy range above 15 kWh on the market, none of the systems are classified as large. S$_{LMO}$ and M$_{NMC}$ systems share similar battery chemistries, but their system design is not comparable. While the M$_{LFP}$ and the M$_{NMC}$ systems show a similar system design, their battery chemistries are not comparable.

The 1,270 monthly CSV files can be downloaded from a public repository[84] (https://doi.org/10.5281/zenodo.12091223).

Field operation of home storage systems

The large dataset allows the information extraction on actual home storage operation (Supplementary Notes 3–5). In the following, the most important findings for method development are presented.

https://doi.org/10.1038/s41560-024-01620-9

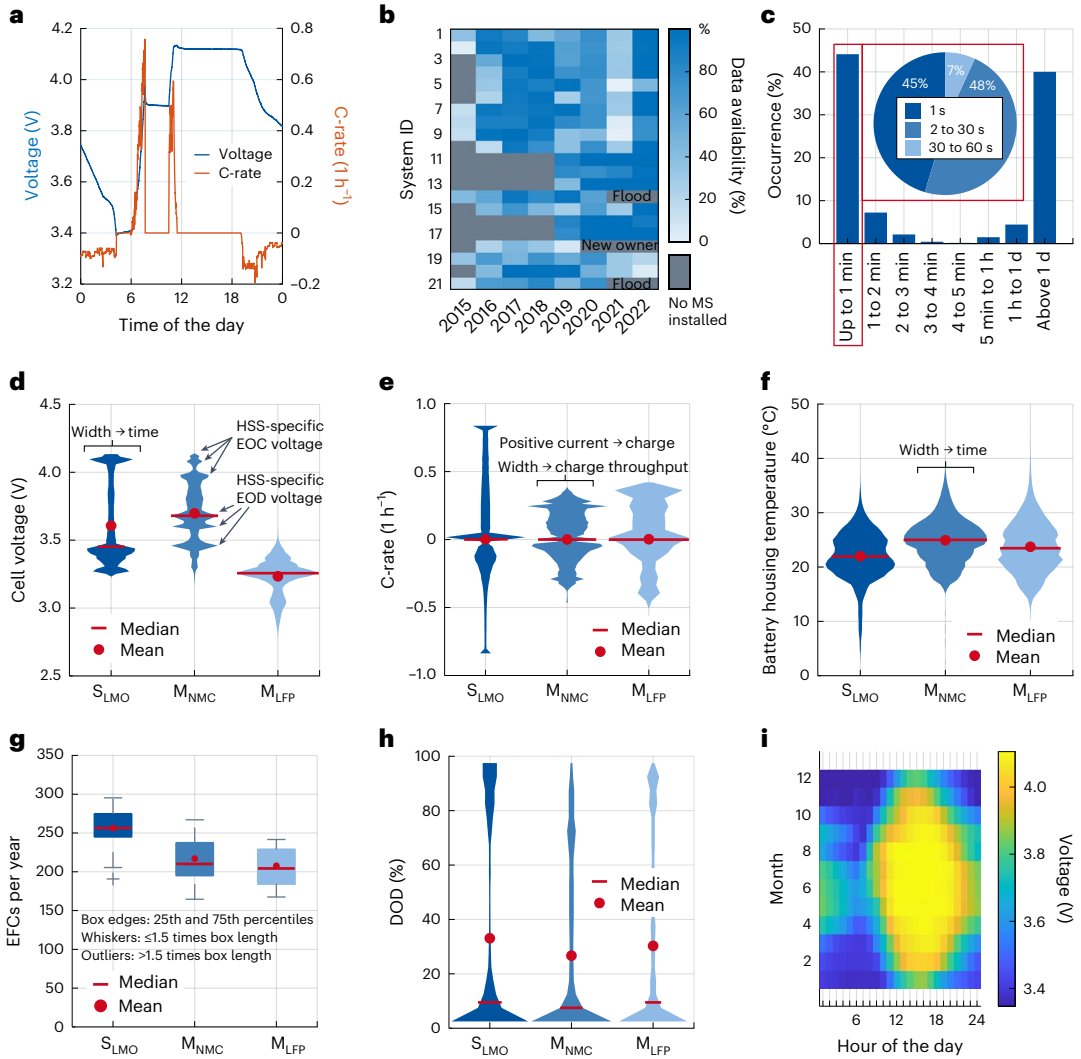


Fig. 1 | Dataset overview. a, Voltage and C-rate over one exemplary day. **b**, Data availability. **c**, Data gap analysis. **d**, Voltage distribution. **e**, Current distribution. **f**, Battery housing temperature. **g**, EFCs per year. **h**, DOD distribution with a bin width of 5 pp and depicted at the midpoint DOD, so DODs close to 0% and 100% are not shown, although they occur. **i**, Mean voltage seasonality.

The HSSs are often fully charged or fully discharged. This can be seen by the wider parts of the violin plots at the top and the bottom of the voltage distribution of the S_{LMO} and M_{NMC} systems in Fig. 1d. The S_{LMO} systems have a clear end of charge (EOC) voltage of around 4.15 V. Their end of discharge (EOD) voltage shows two peaks, as the BMS decreases it over the lifetime to compensate for ageing. The distribution of the M_{NMC} systems shows three peaks each, representing the different EOD and EOC voltages of specific systems with different NMC types and BMS settings. The M_{LFP} distribution does not show the characteristic EOD and EOD peaks owing to the flat OCV of LFP.

The C-rate distributions in Fig. 1e indicate that systems are charged at higher C-rates (positive values) than discharged (negative values). Charging often occurs at higher C-rates owing to the relatively high PV power compared with the battery inverter. By contrast, discharge occurs largely during the night, in which household standby consumption is also met with a few hundred watts, resulting in low discharge rates. The maximum C-rate of an HSS is typically limited by the system design. As the S_{LMO} systems have the highest relative inverter power, their C-rates are higher. However, being a 'small' system is not a general feature of LMO chemistry. There was simply one manufacturer that offered these small battery systems and used LMO batteries by chance.

It is important to note that the parameter distributions of identical systems vary between households as the HSS operation is highly dependent on the PV generation and the electrical house consumption. In addition, the systems show different operational strategies (Supplementary Fig. 1) and different temperature distributions in dependence on the room and the system (Fig. 1f and Supplementary Fig. 2).

Over a year, around 200 EFCs occur for the measured M_{NMC} and M_{LFP} systems, while S_{LMO} systems show yearly values of around 250 EFCs (Fig. 1g). The cycles show clear seasonality with regular full cycles during spring and fall, fewer full cycles during summer and barely any full cycles during winter (Supplementary Figs. 3 and 4). In the summer, some systems are not discharged frequently, and in the winter, some systems do not get fully charged. Figure 1h shows the depth of discharge (DOD) distribution calculated via the rainflow method[85] for the whole operational period. Most DODs are relatively small, with values below 20%. In addition to the small DODs, there are increased values at the upper end of the distribution, with DODs near 100%.

When analysing field data, operational strategies and software updates need to be taken into account. Some of these changes are shown in Supplementary Fig. 5, where the derating behaviour is changed, and the EOD voltage is decreased to counteract battery ageing.

Field capacity tests for method validation

Regular field capacity tests were conducted during the whole measurement period. For this, the HSSs were first fully charged and then

https://doi.org/10.1038/s41560-024-01620-9

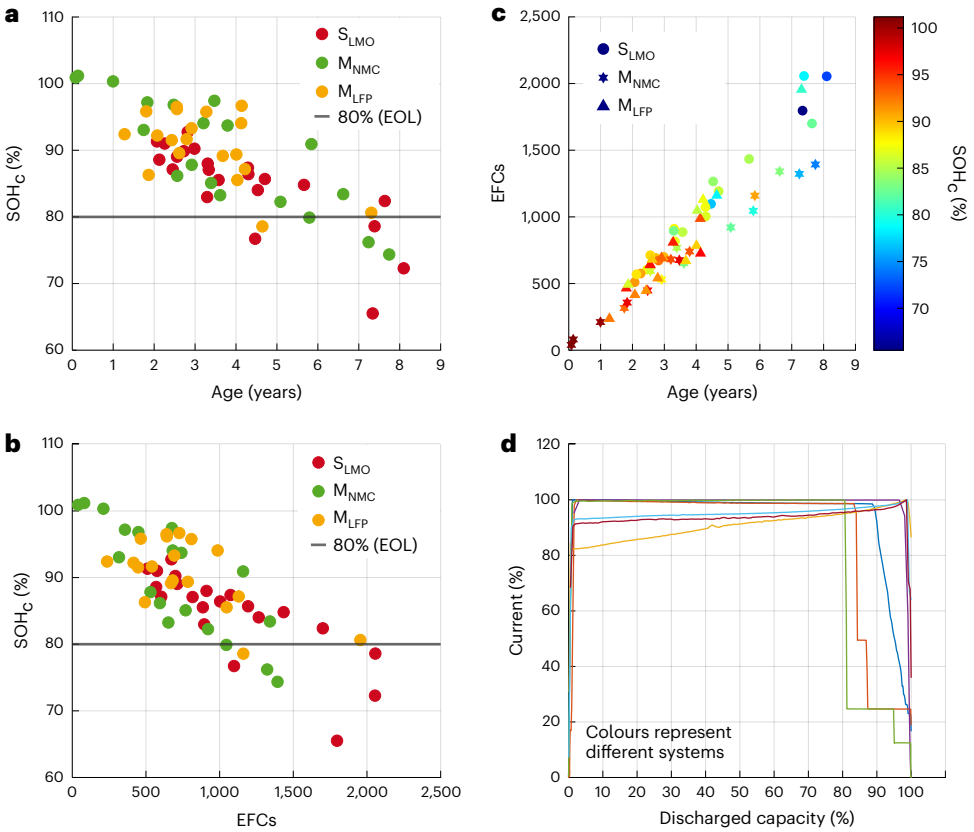


Fig. 2 | Results of the periodic capacity tests for method validation. a, SOH_C over system age. **b**, SOH_C over EFCs. **c**, SOH_C according to age and EFCs. **d**, Different discharge behaviour of HSSs. SOH_C normalized to the nominal capacity stated on the modules.

fully discharged. The discharge was conducted at full power to have a reproducible test scheme in the field. The capacity tests performed have great value. In relation to the research, they validate developed methods such as these within this paper. Such validation is not straightforwardly possible in other studies. In addition, the sheer amount of time required is worth emphasizing. The test preparation, conduction and follow-up take about 2 days on average. The 60 successfully conducted capacity tests alone correspond to a working time of around 120 days.

Figure 2 shows the development of the SOH_C based on the usable capacity over (a) system age, (b) EFCs and (c) both system age and EFCs. Each point corresponds to a manual capacity test. Figure 2d depicts the test current for exemplary HSSs, normalized to its maximum value. It shows the difference between the HSSs' control strategies. While some HSSs have a constant current discharge, others apply a constant power discharge, leading to a rising current. Towards the end of discharge, control strategies from a sharp drop in current to a steady decrease exist, which varies from product to product and even changes with software updates.

The usable capacity decreases over the years. While S_{LMO} HSSs show an average capacity decrease of 2.1 pp per year (a^{-1}), M_{NMC} systems show an average decrease of 3.2 pp a^{-1}, and M_{LFP} systems of 2.2 pp a^{-1} based on the capacity tests. After 7 years, the first end of life (EOL) cases can be identified following the test results, although some tests show slightly lower values than 80% after already 4.5 years. However, the EOL shown in Fig. 2 does not define a warranty case, as datasheets often contain an ageing reserve in their stated value to meet the warranty (Supplementary Note 6).

The EFCs increase approximately linearly over time for the different HSS classifications. The S_{LMO} systems show the most cycles, followed by the medium systems. Nevertheless, one M_{LFP} system reaches a similar number of EFCs as the S_{LMO} systems after more than 7 years (Fig. 2c). Regarding ageing, a capacity fade can be observed for all HSSs. The SOH_C values depend on the specific HSS within a system type. Especially for the older S_{LMO} systems, varying SOH_C results can be observed at a similar age. In addition, the ageing behaviour differs among the system types. The S_{LMO} systems do not show lower SOH_C values compared with the M_{NMC} systems despite more EFCs at a comparable age.

Supplementary Note 6 provides all the necessary information to understand the conducted capacity tests and warranty conditions. Supplementary Fig. 6 explains the capacity reserves that manufacturers apply to meet warranty conditions. The reserves are implemented by stating less capacity on the datasheet than the HSSs have. Supplementary Fig. 7 shows the capacity test scheme, and Supplementary Fig. 8 shows the influence of the ageing reserve and the normalization quantity on the warranty condition.

Capacity estimation based on operational data

HSSs regularly reach EOC and EOD voltage, and full cycles occur. The developed method uses this behaviour to estimate the capacity (Methods and Supplementary Methods). First, it identifies relaxation phases around the EOC and EOD voltages. Second, it estimates the relaxation OCV using a second-order equivalent circuit model with a two-step fitting procedure. Third, it estimates the capacity using an offset-current-corrected coulomb counting between a fully charged (EOC voltage) and a fully discharged (EOD voltage) state.

Figure 3 shows the storage operation of two exemplary days. During this period, the HSS shows a full cycle: It is empty at the beginning of day 1, gets fully charged until noon, stays at a high SOC during the day and is fully discharged overnight. The next day, it gets fully charged again. On the basis of this storage operation, four integration possibilities exist to estimate the capacity while integrating the current

https://doi.org/10.1038/s41560-024-01620-9

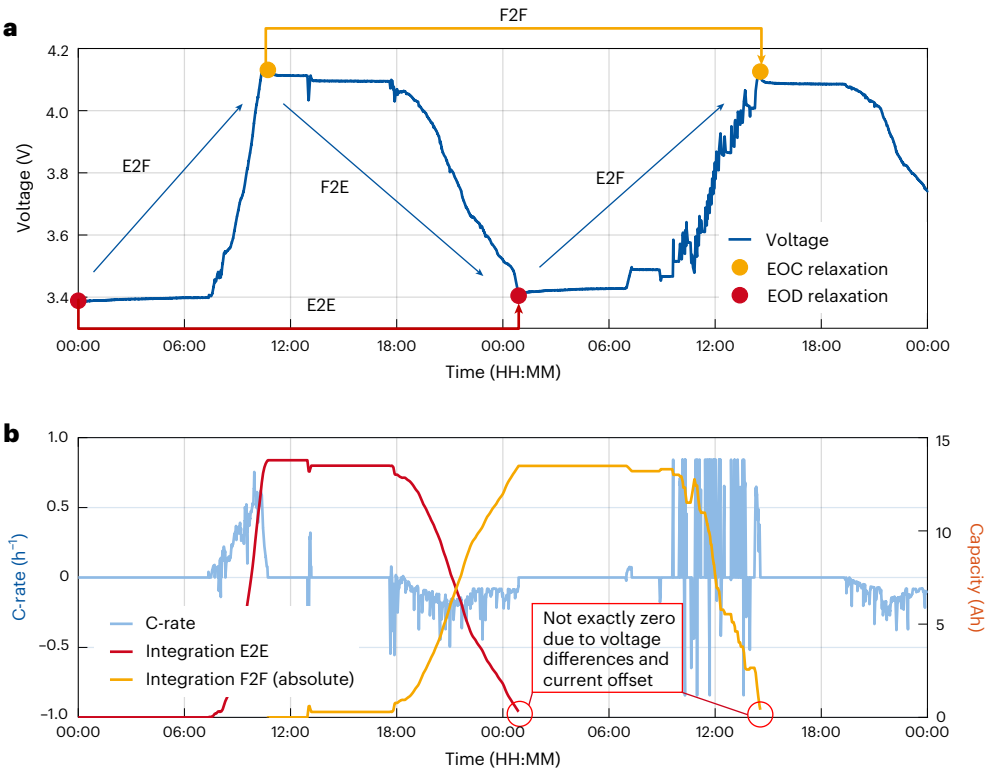


Fig. 3 | Methodology of the capacity estimation based on field measurements of an exemplary S_{LMO} HSS (15 Ah cell). a, Voltage and relaxation points. To identify full cycles, EOC and EOD relaxations can be combined. Full cycles are represented between E2E and F2F. A full charge is represented by E2F and a full discharge by F2E. **b**, C-rate and capacity estimate. The current can be integrated between the identified relaxation points to compute the capacity.

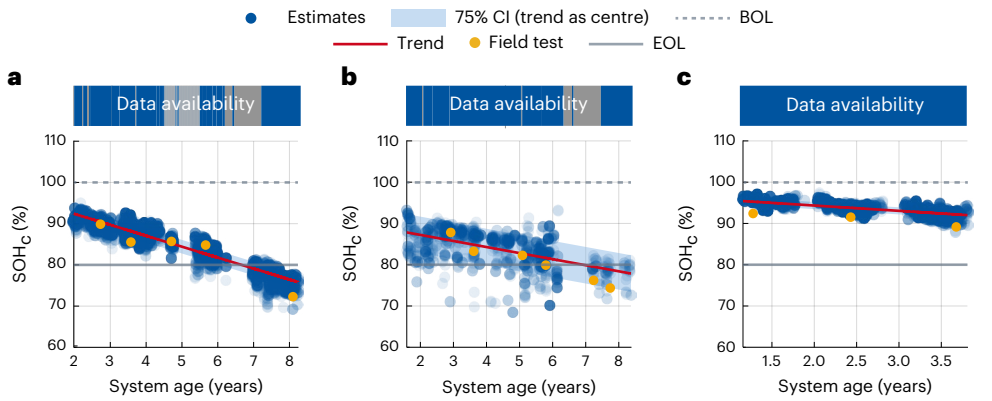


Fig. 4 | SOH_C estimate (normalized to nominal capacity) for three exemplary HSSs. a, S_{LMO}. **b**, M_{NMC}. **c**, M_{LFP}. Estimates validated by field capacity tests. The darker the blue points are, the more estimates exist. The trend is a linear fit of the estimates. The CI of 75% of all estimates is shown in light blue. The measurements started delayed after system commissioning (start of *x*-axis). Beginning of life (BOL) defined as 100%, and EOL defined as 80% of the nominal capacity.

from empty-to-empty (E2E), full-to-full (F2F), empty-to-full (E2F) and full-to-empty (F2E).

When integrating full cycles in the form of E2E and F2F operations, it becomes apparent that the integrated current is not exactly equal to zero. First, the respective start and end points in the form of EOC and EOD voltage are not identical, as these vary during operation. Second, the BMS is also partly supplied by the HSS itself. Next to the BMS power supply, balancing different cell voltages requires energy as well. Therefore, the current is corrected, as presented in Supplementary Methods. In addition, a coulomb-counting SOC estimation that is recalibrated with the regularly occurring EOC or EOD relaxation phases is implemented.

Figure 4 shows the results of the capacity estimate for three exemplary HSSs: (a) S_{LMO}, (b) M_{NMC} and (c) M_{LFP}. While the orange dots represent the manual field capacity tests, the blue dots show the algorithmic capacity estimates. The confidence interval (CI) in light blue contains 75% of all estimates.

As this paper does not focus on ageing fitting methods, a linear fit is applied to the values of the algorithmic capacity estimate, and its gradient is defined as the ageing rate. A linear fit is in line with some observations in literature[86], although both linear and nonlinear ageing behaviour are possible[87]. However, the so-called knee point[88,89] cannot yet be observed clearly for the systems. While the field capacity tests of the S_{LMO} and the M_{NMC} systems vary around the ageing trend, the capacity test values of the M_{LFP} systems are always at the lower end of the estimates and below the trend. The reason for this is that the system does not reduce the current towards the EOD voltage. This results in

https://doi.org/10.1038/s41560-024-01620-9

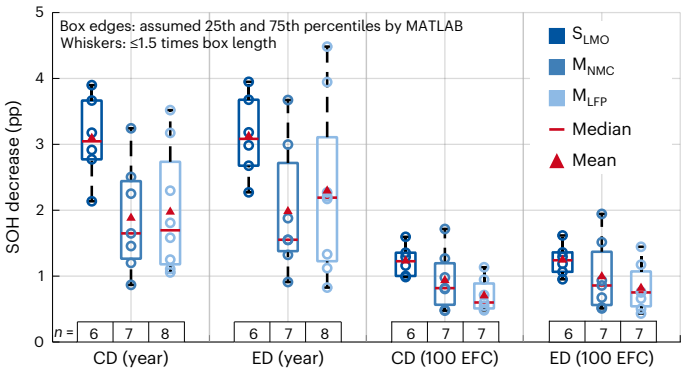


Fig. 5 | Ageing trends of all 21 systems. Decrease in SOH_C (usable capacity decrease (CD)) and SOH_E (usable energy decrease (ED)) per year and per 100 EFCs. The box plot contains the gradient of the linear ageing fit from Fig. 4. Each circle is one system. One M_{LFP} system has too many data outages to estimate the EFCs, which is why there are only seven systems depicted. Box plots are calculated by 'box plot' function of MATLAB, where boxes contain 50% of all values of the assumed distribution.

an earlier reach of EOD owing to overvoltage and a smaller capacity value, because the capacity tests are conducted at maximum C-rate.

Figure 5 provides all ageing rates for the three system types identified by the linear fit for the HSSs both for capacity and energy on an annual basis and per 100 EFCs.

The mean values for the decrease in SOH_C are 3.1 pp a^{-1} for S_{LMO}, 1.9 pp a^{-1} for M_{NMC} and 2 pp a^{-1} for M_{LFP}. Concerning 100 EFCs, the ageing rates are 1.2 pp per 100 EFCs for S_{LMO}, 0.9 pp per 100 EFCs for M_{NMC} and 0.7 pp per 100 EFCs for M_{LFP}. The high SOH_C decrease of S_{LMO} systems can possibly be explained by their higher number of EFCs, higher DODs and higher C-rates compared with the medium systems. However, for the yearly values, a range of approximately 2 pp a^{-1} can be observed for all system types, showing differences in ageing behaviour between similar HSSs. Purely from the gradients, the physical EOL can be estimated after 5 years (for 4 pp a^{-1}) and after 20 years (for 1 pp a^{-1}). While the shorter durations can already be confirmed for some HSSs, linear extrapolation is not reasonable for the HSSs with low ageing rates based on the nonlinear ageing towards the EOL.

The S_{LMO} systems show the lowest mean capacity confidence width with a value of 4.4 pp, followed by the M_{NMC} systems with 6.8 pp and the M_{LFP} systems with 8.0 pp. The reason for the high accuracy of S_{LMO} systems can be explained by their high cycle number and an accurate identification of EOC and EOD voltage owing to the LMO OCV curve. The M_{NMC} systems with NMC cells share this voltage characteristic but show fewer full cycles, leading to fewer estimates and, consequently, wider confidence ranges. In addition, a higher connection of cells in parallel leads to higher inaccuracy in OCV estimation for some systems while others can be estimated with higher accuracy. LFP has a substantially flatter OCV curve than LMO and NMC, leading to less accurate EOC and EOD detection. Combined with a medium number of full cycles, their average usable capacity and energy estimates are worse, although some systems reach comparably good CI values below 5%.

The results for the usable energy decrease look similar to the capacity analysis, leading to the conclusion that the loss of capacity is the dominant ageing effect. A possible increase in internal resistance appears secondary. Otherwise, the decrease in energy-related state of health (SOH_E) would be significantly higher owing to resistance losses.

An offset-corrected coulomb counting is described as an established method in literature with known shortcomings of error accumulation and unknown start SOC. In addition, manufacturers have already applied the method. However, we think that the following arguments highlight the importance of the presented method, which is tailored to HSS operation. First, the regular and timely close reach of EOD and EOC voltage of HSSs ensures that error accumulation is limited, and the SOC can be recalibrated frequently. This focus on regularly occurring full cycles is not possible for many other applications such as EVs (which typically do not get fully discharged) or battery storage systems for frequency restoration (which have a mean SOC of around 50%). Further, the applied current correction makes the errors smaller. Second, the capacity estimation method does not require an initial SOC, as it starts and ends at fully charged or fully discharged states close to the identified EOD and EOC voltage. Third, literature describes the method as state-of-the-art. However, we still see industry field data analyses with inaccurate SOH estimates not being the exception. To us, there is a gap between literature statements and especially smaller manufacturers' implementation state. Our method shows how to adapt an established method to the specifics of HSS operation, offering an approach that needs to store only the data of full cycles occurring in normal operation. We consider the method robust, as it works for system-level field data of three relevant lithium-ion technologies without knowing all exact battery cells or having manufacturer OCV curves. Thus, it can also be used by external companies to help customers with warranty claims. The rather simple methodology makes the method transparent to all parties involved.

Conclusion

The batteries regulation of the European Union[4] requires reliable SOH estimation based on field data. However, so far, neither standardized methods nor enough datasets exist to develop these. This paper contributes to both by analysing field measurements of 21 HSSs over a measurement period of up to 8 years. The dataset is, so far, valuable for a scientific dataset in terms of measurement duration and sample rate. It consists of 106 system years represented by 14 billion data points. Its 146 gigabytes cover three important lithium-ion battery technologies: LFP, NMC and a blend of LMO and NMC.

The developed SOH estimation automatically detects the electrochemical processes of overvoltage relaxation at low currents and uses their characteristics for the parameter estimation of a second-order equivalent circuit battery model. With these parameters, the exact SOC at both full charge and full discharge is calculated. These values compute the remaining capacity, energy and SOH while analysing current and voltage using coulomb counting and current correction. The analysed storage systems show average decreases in usable capacity of around two to three percentage points per year. From a technical perspective, single systems with a higher capacity fade reach their EOL after 5–7 years, defined as 80% of their nominal capacity. Others still show reasonable SOH values after the same operational period, indicating a longer lifetime. Nevertheless, the given warranty periods can be reached in most cases by including ageing reserves. Considering that the measured HSSs were from the first product generation, this is a positive sign for the industry.

Methods

Battery model and relaxation phase detection

A battery model is needed to estimate the OCV of the battery at identified EOC and EOD relaxation phases. The used second-order battery model is inspired by literature[90–93], and its parametrization is described in Supplementary Methods (Supplementary Figs. 9–11, with Supplementary equations (1)–(5)).

Equation (1) is used for the final fit. The parameters include the measured battery voltage V_{bat}, the open circuit voltage V_{OCV}, the voltage V_{fast} over the first resistor-capacitor (RC) element for the fast processes like charge transfer with the time constant τ_{fast}, and the voltage V_{slow} over the second RC element responsible for slow diffusion effects with the time constant τ_{slow}. The distribution of the relaxation voltages and their durations can be seen in Supplementary Fig. 12.

$$V_{bat}(t) - V_{OCV} = V_{fast} \times e^{\frac{-t^+}{\tau_{fast}}} + V_{slow} \times e^{\frac{-t^+}{\tau_{slow}}}$$
$$\text{with } \tau_{fast_{min}} \le \tau_{fast} \le \tau_{fast_{max}} \text{ and } \tau_{slow_{min}} \le \tau_{slow} \le \tau_{slow_{max}} \quad (1)$$

SOC calculation and current correction

The SOC is calculated using equation (2). The reasonably constant energy supply of the battery to the BMS and regular balancing activities lead to an error in SOC estimation. The reason for this is that the measurement system is attached to the DC poles of the whole HSS's battery. Thus, the internal energy supply of the BMS and balancing activities are not measured directly, possibly leading to offsets. The whole current correction is explained in Supplementary Methods (Supplementary Figs. 13 and 14). The parameters include the battery current I_{bat}, the offset current I_{offset} and the usable capacity C_{usable}:

$$\mathrm{SOC}(t) = \mathrm{SOC}(t_0) + \frac{\int_{t_0}^{t_0+t} (I_{bat}(t) - I_{offset}(t))dt}{C_{usable}(t)} \quad (2)$$

SOH calculation

The SOH_C serves as an indicator of a battery's ageing conditions and limitations set by the BMS. It is derived from the ratio between the remaining usable capacity C_{usable} and its nominal capacity $C_{nominal}$, as represented in equation (3)[94]:

$$\mathrm{SOH_C}(t) = \frac{C_{usable}(t)}{C_{nominal}} \quad (3)$$

Data availability

The 1,270 monthly CSV files can be downloaded from the following repository hosted by Zenodo: https://doi.org/10.5281/zenodo.12091223 (ref. 84). Source data are provided with this paper.

Code availability

Code to work with the data can be downloaded from the following repository hosted by Zenodo: https://doi.org/10.5281/zenodo.12091223 (ref. 84).

References

1. Figgener, J. et al. The development of stationary battery storage systems in Germany—A market review. *J. Energy Storage* **29**, 101153 (2020).
2. Pozzato, G. et al. Analysis and key findings from real-world electric vehicle field data. *Joule* https://doi.org/10.1016/j.joule.2023.07.018 (2023).
3. Jacqué, K., Koltermann, L., Figgener, J., Zurmühlen, S. & Sauer, D. U. The influence of frequency containment reserve on the operational data and the state of health of the hybrid stationary large-scale storage system. *Energies* **15**, 1342 (2022).
4. *Regulation (EU) 2023/1542 of the European Parliament and of the Council of 12 July 2023 Concerning Batteries and Waste Batteries, Amending Directive 2008/98/EC and Regulation (EU) 2019/1020 and Repealing Directive 2006/66/EC* (European Commission, 2023); https://eur-lex.europa.eu/legal-content/EN/TXT/?uri=CELEX:02006L0066-20180704
5. Ecker, M. et al. Calendar and cycle life study of Li(NiMnCo)O_2-based 18650 lithium-ion batteries. *J. Power Sources* **248**, 839–851 (2014).
6. Baumhöfer, T., Brühl, M., Rothgang, S. & Sauer, D. U. Production caused variation in capacity aging trend and correlation to initial cell performance. *J. Power Sources* **247**, 332–338 (2014).
7. Liu, S. et al. Analysis of cyclic aging performance of commercial $Li_4Ti_5O_{12}$-based batteries at room temperature. *Energy* **173**, 1041–1053 (2019).
8. Harlow, J. E. et al. A wide range of testing results on an excellent lithium-ion cell chemistry to be used as benchmarks for new battery technologies. *J. Electrochem. Soc.* **166**, A3031–A3044 (2019).
9. Glazier, S. L., Li, J., Louli, A. J., Allen, J. P. & Dahn, J. R. An analysis of artificial and natural graphite in lithium ion pouch cells using ultra-high precision coulometry, isothermal microcalorimetry, gas evolution, long term cycling and pressure measurements. *J. Electrochem. Soc.* **164**, A3545–A3555 (2017).
10. Ma, X. et al. Editors' choice—hindering rollover failure of $Li[Ni_{0.5}Mn_{0.3}Co_{0.2}]O_2$/graphite pouch cells during long-term cycling. *J. Electrochem. Soc.* https://doi.org/10.1149/2.0801904jes (2019).
11. Severson, K. A. et al. Data-driven prediction of battery cycle life before capacity degradation. *Nat. Energy* **4**, 383–391 (2019).
12. Preger, Y. et al. Degradation of commercial lithium-ion cells as a function of chemistry and cycling conditions. *J. Electrochem. Soc.* **167**, 120532 (2020).
13. Devie, A., Baure, G. & Dubarry, M. Intrinsic variability in the degradation of a batch of commercial 18650 lithium-ion cells. *Energies* **11**, 1031 (2018).
14. Zhang, Y. et al. Identifying degradation patterns of lithium ion batteries from impedance spectroscopy using machine learning. *Nat. Commun.* **11**, 1706 (2020).
15. Lewerenz, M., Fuchs, G., Becker, L. & Sauer, D. U. Irreversible calendar aging and quantification of the reversible capacity loss caused by anode overhang. *J. Energy Storage* **18**, 149–159 (2018).
16. Schmalstieg, J., Kabitz, S., Ecker, M. & Sauer, D. U. From accelerated aging tests to a lifetime prediction model: analyzing lithium-ion batteries. In *2013 World Electric Vehicle Symposium and Exhibition (EVS27)* 370– 381 (IEEE, 2013).
17. Woody, M., Arbabzadeh, M., Lewis, G. M., Keoleian, G. A. & Stefanopoulou, A. Strategies to limit degradation and maximize Li-ion battery service lifetime—critical review and guidance for stakeholders. *J. Energy Storage* **28**, 101231 (2020).
18. Lewerenz, M. et al. Systematic aging of commercial $LiFePO_4$|graphite cylindrical cells including a theory explaining rise of capacity during aging. *J. Power Sources* **345**, 254–263 (2017).
19. Deline, C. et al. Field-aging test bed for behind-the-meter PV + energy storage. In *2019 IEEE 46th Photovoltaic Specialists Conference (PVSC)* 1341–1345 (IEEE, 2019).
20. Benato, R., Dambone Sessa, S., Musio, M., Palone, F. & Polito, R. Italian experience on electrical storage ageing for primary frequency regulation. *Energies* **11**, 2087 (2018).
21. Elliott, M., Swan, L. G., Dubarry, M. & Baure, G. Degradation of electric vehicle lithium-ion batteries in electricity grid services. *J. Energy Storage* **32**, 101873 (2020).
22. *Lithium-Ion Battery Testing* Public Report 9 (ITP Renewables, 2020); https://batterytestcentre.com.au/reports/
23. Dubarry, M. et al. Battery energy storage system battery durability and reliability under electric utility grid operations: analysis of 3 years of real usage. *J. Power Sources* **338**, 65–73 (2017).
24. Dubarry, M., Tun, M., Baure, G., Matsuura, M. & Rocheleau, R. E. Battery durability and reliability under electric utility grid operations: analysis of on-site reference tests. *Electronics* **10**, 1593 (2021).
25. Kubiak, P., Cen, Z., López, C. M. & Belharouak, I. Calendar aging of a 250 kW/500 kWh Li-ion battery deployed for the grid storage application. *J. Power Sources* **372**, 16–23 (2017).
26. Hund, T. D. & Gates, S. PV hybrid system and battery test results from Grasmere Idaho. In *Conference Record of 29th IEEE Photovoltaic Specialists Conference* 1424–1427 (IEEE, 2002).
27. Gustavsson, M. & Mtonga, D. Lead-acid battery capacity in solar home systems—field tests and experiences in Lundazi, Zambia. *Sol. Energy* **79**, 551–558 (2005).
28. Lansburg, S., Brenier, A. & Boulais, R. Passing the 10-year mark—a multi-year, multi-technology analysis of Ni-Cd field data. In *International Conference on Telecommunications Energy (INTELEC)* 400–407 (IEEE, 2010).

29. Schaeck, S., Karspeck, T., Ott, C., Weckler, M. & Stoermer, A. O. A field operational test on valve-regulated lead-acid absorbent-glass-mat batteries in micro-hybrid electric vehicles. Part I. Results based on kernel density estimation. *J. Power Sources* **196**, 2924–2932 (2011).
30. Calearo, L., Ziras, C., Thingvad, A. & Marinelli, M. Agnostic battery management system capacity estimation for electric vehicles. *Energies* **15**, 9656 (2022).
31. Kim, S. K., Cho, K. H., Kim, J. Y. & Byeon, G. Field study on operational performance and economics of lithium-polymer and lead-acid battery systems for consumer load management. *Renew. Sustain. Energy Rev.* **113**, 109234 (2019).
32. Xu, Z., Wang, J., Lund, P. D. & Zhang, Y. Estimation and prediction of state of health of electric vehicle batteries using discrete incremental capacity analysis based on real driving data. *Energy* **225**, 120160 (2021).
33. Zhang, Q. et al. State-of-health estimation of batteries in an energy storage system based on the actual operating parameters. *J. Power Sources* **506**, 230162 (2021).
34. Abedi Varnosfaderani, M., Strickland, D., Ruse, M. & Brana Castillo, E. Sweat testing cycles of batteries for different electrical power applications. *IEEE Access* **7**, 132333–132342 (2019).
35. Jannati, M. & Foroutan, E. Analysis of power allocation strategies in the smoothing of wind farm power fluctuations considering lifetime extension of BESS units. *J. Clean. Prod.* **266**, 122045 (2020).
36. Karoui, F. et al. Diagnosis and prognosis of complex energy storage systems: tools development and feedback on four installed systems. *Energy Procedia* **155**, 61–76 (2018).
37. Koller, M., Borsche, T., Ulbig, A. & Andersson, G. Review of grid applications with the Zurich 1 MW battery energy storage system. *Electr. Power Syst. Res.* **120**, 128–135 (2015).
38. Münderlein, J., Steinhoff, M., Zurmühlen, S. & Sauer, D. U. Analysis and evaluation of operations strategies based on a large scale 5 MW and 5 MWh battery storage system. *J. Energy Storage* **24**, 100778 (2019).
39. Li, W. et al. Online capacity estimation of lithium-ion batteries with deep long short-term memory networks. *J. Power Sources* **482**, 228863 (2021).
40. Xu, J., Cao, B., Chen, Z. & Zou, Z. An online state of charge estimation method with reduced prior battery testing information. *Int. J. Electr. Power Energy Syst.* **63**, 178–184 (2014).
41. How, D. N. T., Hannan, M. A., Hossain Lipu, M. S. & Ker, P. J. State of charge estimation for lithium-ion batteries using model-based and data-driven methods: a review. *IEEE Access* **7**, 136116–136136 (2019).
42. Wang, Z., Feng, G., Zhen, D., Gu, F. & Ball, A. A review on online state of charge and state of health estimation for lithium-ion batteries in electric vehicles. *Energy Rep.* **7**, 5141–5161 (2021).
43. Yu, Q., Xiong, R., Yang, R. & Pecht, M. G. Online capacity estimation for lithium-ion batteries through joint estimation method. *Appl. Energy* **255**, 113817 (2019).
44. Kim, T. et al. A real-time condition monitoring for lithium-ion batteries using a low-price microcontroller. In *2017 IEEE Energy Conversion Congress and Exposition (ECCE)* 5248–5253 (IEEE, 2017).
45. Kim, T. et al. An on-board model-based condition monitoring for lithium-ion batteries. *IEEE Trans. Ind. Appl.* **55**, 1835–1843 (2019).
46. Wang, Y., Gao, G., Li, X. & Chen, Z. A fractional-order model-based state estimation approach for lithium-ion battery and ultra-capacitor hybrid power source system considering load trajectory. *J. Power Sources* **449**, 227543 (2020).
47. Li, W. et al. Electrochemical model-based state estimation for lithium-ion batteries with adaptive unscented Kalman filter. *J. Power Sources* **476**, 228534 (2020).
48. Marcicki, J., Todeschini, F., Onori, S. & Canova, M. Nonlinear parameter estimation for capacity fade in lithium-ion cells based on a reduced-order electrochemical model. In *American Control Conference* 572–577 (IEEE, 2012).
49. Doyle, M., Fuller, T. F. & Newman, J. Modeling of galvanostatic charge and discharge of the lithium/polymer/insertion cell. *J. Electrochem. Soc.* **140**, 1526–1533 (1993).
50. Fuller, T. F., Doyle, M. & Newman, J. Simulation and optimization of the dual lithium ion insertion cell. *J. Electrochem. Soc.* **141**, 1–10 (1994).
51. Xiong, R., Li, L. & Tian, J. Towards a smarter battery management system: a critical review on battery state of health monitoring methods. *J. Power Sources* **405**, 18–29 (2018).
52. Richardson, R. R., Birkl, C. R., Osborne, M. A. & Howey, D. A. Gaussian process regression for in situ capacity estimation of lithium-ion batteries. *IEEE Trans. Ind. Inf.* **15**, 127–138 (2019).
53. Yang, D., Zhang, X., Pan, R., Wang, Y. & Chen, Z. A novel Gaussian process regression model for state-of-health estimation of lithium-ion battery using charging curve. *J. Power Sources* **384**, 387–395 (2018).
54. Wei, J., Dong, G. & Chen, Z. Remaining useful life prediction and state of health diagnosis for lithium-ion batteries using particle filter and support vector regression. *IEEE Trans. Ind. Electron.* **65**, 5634–5643 (2018).
55. Klass, V., Behm, M. & Lindbergh, G. A support vector machine-based state-of-health estimation method for lithium-ion batteries under electric vehicle operation. *J. Power Sources* **270**, 262–272 (2014).
56. Chemali, E., Kollmeyer, P. J., Preindl, M., Ahmed, R. & Emadi, A. Long short-term memory networks for accurate state-of-charge estimation of Li-ion batteries. *IEEE Trans. Ind. Electron.* **65**, 6730–6739 (2018).
57. Shen, S., Sadoughi, M., Chen, X., Hong, M. & Hu, C. A deep learning method for online capacity estimation of lithium-ion batteries. *J. Energy Storage* **25**, 100817 (2019).
58. Chaoui, H. & Ibe-Ekeocha, C. C. State of charge and state of health estimation for lithium batteries using recurrent neural networks. *IEEE Trans. Veh. Technol.* **66**, 8773–8783 (2017).
59. dos Reis, G., Strange, C., Yadav, M. & Li, S. Lithium-ion battery data and where to find it. *Energy AI* **5**, 100081 (2021).
60. Dubarry, M., Costa, N. & Matthews, D. Data-driven direct diagnosis of Li-ion batteries connected to photovoltaics. *Nat. Commun.* **14**, 3138 (2023).
61. Dubarry, M., Yasir, F., Costa, N. & Matthews, D. Data-driven diagnosis of PV-connected batteries: analysis of two years of observed irradiance. *Batteries* **9**, 395 (2023).
62. Attia, P. M. et al. Closed-loop optimization of fast-charging protocols for batteries with machine learning. *Nature* **578**, 397–402 (2020).
63. Saha, B. & Goebel, K. Battery data set https://www.nasa.gov/intelligent-systems-division/discovery-and-systems-health/pcoe/pcoe-data-set-repository/ (2007).
64. Battery data. *Center for Advanced Life Cycle Engineering (CALCE)* https://calce.umd.edu/battery-data (2024).
65. Juarez Robles, D., Jeevarajan, J. A. & Mukherjee, P. P. Aging test - cylindrical cell - part 01 - single cells. *Zenodo* https://doi.org/10.5281/zenodo.4443455 (2021).
66. Catenaro, E. & Onori, S. Experimental data of three lithium-ion batteries under galvanostatic discharge tests at different C-rates and operating temperatures. *Mendeley Data* https://doi.org/10.17632/KXSBR4X3J2.2 (2021).
67. Birkl, C. & Howey, D. Oxford battery degradation dataset 1. *Univ. Oxford* https://doi.org/10.5287/bodleian:KO2kdmYGg (2017).
68. Kollmeyer, P. Panasonic 18650PF Li-ion battery data. *Mendeley Data* https://doi.org/10.17632/wykht8y7tg.1 (2018).

69. Luzi, M. Automotive Li-ion cell usage data set. *IEEEDataPort* https://doi.org/10.21227/ce9q-jr19 (2022).
70. Wang, Y., Liu, C., Pan, R. & Chen, Z. Experimental data of lithium-ion battery and ultracapacitor under DST and UDDS profiles at room temperature. *Data Brief* **12**, 161–163 (2017).
71. Pozzato, G. et al. Real-world electric vehicle data: driving and charging. *Mendeley Data* https://doi.org/10.17632/7vdkzpnjgj.2 (2023).
72. Dubarry, M. Graphite//LFP synthetic training prognosis dataset. *Mendeley Data* https://doi.org/10.17632/6s6ph9n8zg.1 (2020).
73. Dubarry, M. & Beck, D. Analysis of synthetic voltage vs. capacity datasets for big data Li-ion diagnosis and prognosis. *Energies* **14**, 2371 (2021).
74. Rücker, F., Figgener, J., Schoeneberger, I. & Sauer, D. U. Battery electric vehicles in commercial fleets: use profiles, battery aging, and open-access data. *J. Energy Storage* **86**, 111030 (2024).
75. Rücker, F., Figgener, J., Schoeneberger, I. & Sauer, D. U. Dataset to 'Battery electric vehicles in commercial fleets: use profiles, battery aging, and open-access data'. *RWTH Aachen Univ.* https://doi.org/10.18154/RWTH-2024-01907 (2024).
76. Aitio, A. & Howey, D. A. Predicting battery end of life from solar off-grid system field data using machine learning. *Joule* **5**, 3204–3220 (2021).
77. Wang, Q. et al. Large-scale field data-based battery aging prediction driven by statistical features and machine learning. *Cell Rep. Phys. Sci.* https://doi.org/10.1016/j.xcrp.2023.101720 (2023).
78. Song, L., Zhang, K., Liang, T., Han, X. & Zhang, Y. Intelligent state of health estimation for lithium-ion battery pack based on big data analysis. *J. Energy Storage* **32**, 101836 (2020).
79. He, Z. et al. State-of-health estimation based on real data of electric vehicles concerning user behavior. *J. Energy Storage* **41**, 102867 (2021).
80. She, C., Wang, Z., Sun, F., Liu, P. & Zhang, L. Battery aging assessment for real-world electric buses based on incremental capacity analysis and radial basis function neural network. *IEEE Trans. Ind. Inf.* **16**, 3345–3354 (2020).
81. Wang, Q., Wang, Z., Zhang, L., Liu, P. & Zhang, Z. A novel consistency evaluation method for series-connected battery systems based on real-world operation data. *IEEE Trans. Transp. Electrific.* **7**, 437–451 (2021).
82. Zhang, Y., Wik, T., Bergström, J., Pecht, M. & Zou, C. A machine learning-based framework for online prediction of battery ageing trajectory and lifetime using histogram data. *J. Power Sources* **526**, 231110 (2022).
83. Huo, Q., Ma, Z., Zhao, X., Zhang, T. & Zhang, Y. Bayesian network based state-of-health estimation for battery on electric vehicle application and its validation through real-world data. *IEEE Access* **9**, 11328–11341 (2021).
84. Figgener, J. et al. Data for: Multi-year field measurements of home storage systems and their use in capacity estimation. *Zenodo* https://doi.org/10.5281/zenodo.12091223 (2024).
85. Xu, B., Oudalov, A., Ulbig, A., Andersson, G. & Kirschen, D. S. Modeling of lithium-ion battery degradation for cell life assessment. *IEEE Trans. Smart Grid* **9**, 1131–1140 (2018).
86. Vermeer, W., Chandra Mouli, G. R. & Bauer, P. A comprehensive review on the characteristics and modeling of lithium-ion battery aging. *IEEE Trans. Transp. Electrific.* **8**, 2205–2232 (2022).
87. Keil, J. et al. Linear and nonlinear aging of lithium-ion cells investigated by electrochemical analysis and in-situ neutron diffraction. *J. Electrochem. Soc.* **166**, A3908–A3917 (2019).
88. Attia, P. M. et al. Review—'Knees' in lithium-ion battery aging trajectories. *J. Electrochem. Soc.* **169**, 60517 (2022).
89. Diao, W., Kim, J., Azarian, M. H. & Pecht, M. Degradation modes and mechanisms analysis of lithium-ion batteries with knee points. *Electrochim. Acta* **431**, 141143 (2022).
90. Bernardi, D. M. & Go, J.-Y. Analysis of pulse and relaxation behavior in lithium-ion batteries. *J. Power Sources* **196**, 412–427 (2011).
91. Pei, L., Wang, T., Lu, R. & Zhu, C. Development of a voltage relaxation model for rapid open-circuit voltage prediction in lithium-ion batteries. *J. Power Sources* **253**, 412–418 (2014).
92. Stroe, A.-I., Stroe, D.-I., Swierczynski, M., Teodorescu, R. & Kaer, S. K. Lithium-ion battery dynamic model for wide range of operating conditions. In *2017 International Conference on Optimization of Electrical and Electronic Equipment (OPTIM) & 2017 Intl Aegean Conference on Electrical Machines and Power Electronics (ACEMP)* 660–666 (IEEE, 2017).
93. Qian, K. et al. State-of-health (SOH) evaluation on lithium-ion battery by simulating the voltage relaxation curves. *Electrochim. Acta* **303**, 183–191 (2019).
94. Sauer, D. U. et al. State of charge—what do we really speak about? *ResearchGate* https://www.researchgate.net/publication/287336237_State_of_charge_-_What_do_we_really_speak_about (1999).

Acknowledgements

Parts of the results were obtained within the research projects 'WMEP PV-Speicher' (funding number 0325666) and 'WMEP PV-Speicher 2.0 (KfW 275)' (funding number 03ET6117), both funded by the German Federal Ministry for Economic Affairs and Climate Action (BMWK), and 'Betterbat' (funding number 03XP0362B), funded by the Federal Ministry of Education and Research (BMBF). We are very thankful to the households that enabled the measurements.

Author contributions

Overall, J.F. led the research during his dissertation on home storage. J.F., D.H., K.-P.K., O.W. and D.U.S. conceptualized the research, planned and conducted the field measurements. J.F., D.H. and J.B. processed the dataset. J.F., J.v.O., D.H., J.B. and P.W. developed the methodology, while M.M., O.W., F.H., C.H., K.-P.K. and D.U.S. supported during this task. J.F., J.v.O., J.B., P.W., D.H. and M.M. developed software to analyse and evaluate the data. J.F. wrote the original paper draft and created the figures and tables with support from J.B., J.v.O. and P.W., while D.H., M.M., C.H. and D.U.S. reviewed and edited the paper. J.F. and D.U.S. supervised the research. J.F., K.-P.K. and D.U.S. did the main funding acquisition and project administration for RWTH Aachen University.

Competing interests

As stated in the paper, the authors J.F., J.v.O., D.H., J.B., M.M., K.-P.K. and D.U.S. are shareholders and/or employees of ACCURE Battery Intelligence GmbH, which offers commercial battery diagnostics. The company is a spin-off of RWTH Aachen University, where the research was conducted. The other authors declare no competing interests.

Additional information

Supplementary information The online version contains supplementary material available at https://doi.org/10.1038/s41560-024-01620-9.

Correspondence and requests for materials should be addressed to Jan Figgener.

Peer review information *Nature Energy* thanks Anirudh Allam and Matthieu Dubarry for their contribution to the peer review of this work.

Reprints and permissions information is available at www.nature.com/reprints.

Publisher's note Springer Nature remains neutral with regard to jurisdictional claims in published maps and institutional affiliations.

Open Access This article is licensed under a Creative Commons Attribution-NonCommercial-NoDerivatives 4.0 International License, which permits any non-commercial use, sharing, distribution and reproduction in any medium or format, as long as you give appropriate credit to the original author(s) and the source, provide a link to the Creative Commons licence, and indicate if you modified the licensed material. You do not have permission under this licence to share adapted material derived from this article or parts of it. The images or other third party material in this article are included in the article's Creative Commons licence, unless indicated otherwise in a credit line to the material. If material is not included in the article's Creative Commons licence and your intended use is not permitted by statutory regulation or exceeds the permitted use, you will need to obtain permission directly from the copyright holder. To view a copy of this licence, visit http://creativecommons.org/licenses/by-nc-nd/4.0/.

© The Author(s) 2024